Review

Recent Advances in Non-Linear Imaging Techniques for Cancer Detection

Francisco J. Ávila *

Posted Date: 19 July 2024

doi: 10.20944/preprints202407.1569.v1

Keywords: Cancer; tumor tissue; microwave imaging; two-photon excitation; second harmonic generation; third harmonic generation; Raman Scattering; Life-time two photon fluorescence; two-photon photodynamic therapy

Review

Recent Advances in Non-Linear Imaging Techniques for Cancer Detection

Francisco J. Ávila

Departamento de Física Aplicada, Facultad de Ciencias, Universidad de Zaragoza, 50009, Spain; avila@unizar.es.

Abstract: The World Health Organization (WHO) cancer agency predicts that more than 35 million cases of will be experienced in 2050, a 77 % increase over the 2022 estimate. Currently, the leading cancer diagnosed cancer are breast, lung and colorectal. There is no standardized tool for cancer diagnosis; initially clinical procedures are guided by the patient's symptoms and generally involve biochemical blood tests, imaging and biopsy. Label-free nonlinear optical approaches are promising tool for tumor imaging, due to their inherent non-invasive biosafe contrast mechanisms and the ability to monitor collagen-related disorders and metabolic changes during cancer progression. Last advances in nonlinear modalities for tumor imaging are reviewed here. In addition, an application of a blind deconvolution procedure to improve the quality of two-photon images of breast tumor tissues is shown.

Keywords: cancer; tumor tissue; microwave imaging; two-photon excitation; second harmonic generation; third harmonic generation; Raman Scattering; Life-time two photon fluorescence; two-photon photodynamic therapy

1. Introduction

The survival probity of patients mainly depends on the early detection, cancer type, treatments outcomes and genetic factors [1]. Tumor markers help diagnose the type and stage of cancer, and to decide what treatment might be effective. Tumor markers also inform about the aggressiveness, whether the treatment is being effective or if cancer has returned. However, tumor markers are not universal to each type of cancer, and the same type of tumor marker can show unpaired expression levels even in two patients underlying the same stage and type of cancer.

In contrast, cancer cells share common characteristics such as activation, metabolism and dynamic nuclear activity [2]. Tumors require a microenvironment conducive to tumorigenesis. As a consequence, the extracellular matrix undergoes remodeling through cell-tumor matrix interaction that favors progression and metastasis [3].

In this review, major advances in non-linear optical imaging modalities that provide electrical, chemical, structural and metabolic information about tumor tissues are discussed. Furthermore, as a complementary supporting tool to enhance the analysis of tumor tissues imaging, a digital processing procedure based on blind image restoration is tested on two-photon fluorescence microscopy images from breast tumor tissues.

2. Microwave Tomographic Imaging

Microwave tomographic imaging (MTI) technique is based on non-ionizing electromagnetic radiation in microwave regime (range of 200 MHz-300 GHz) to obtain information about an object hidden within a structure (or a biological medium) [4]. The penetrating power of microwaves into biological samples makes this technique useful for biomedical applications such as tomographic imaging. The microwaves penetration depends on the electrical and magnetic properties of the analyzed sample [5].

 doi:10.20944/preprints202407.1569.v1

The physical basics of microwave imaging consist of illuminating biological tissue with ultra-wideband pulses from transmitting antennas and then processing the coherent addition of reflections from scattered objects of interest. The detection configuration based on antenna arrays together with inverse image formation algorithms allows detection of small lesions (less than 1 cm) with three-dimensional confocal resolution [6]. The physical interface for performing microwave imaging is a vector network analyzer [7] as schematized in Figure 1.

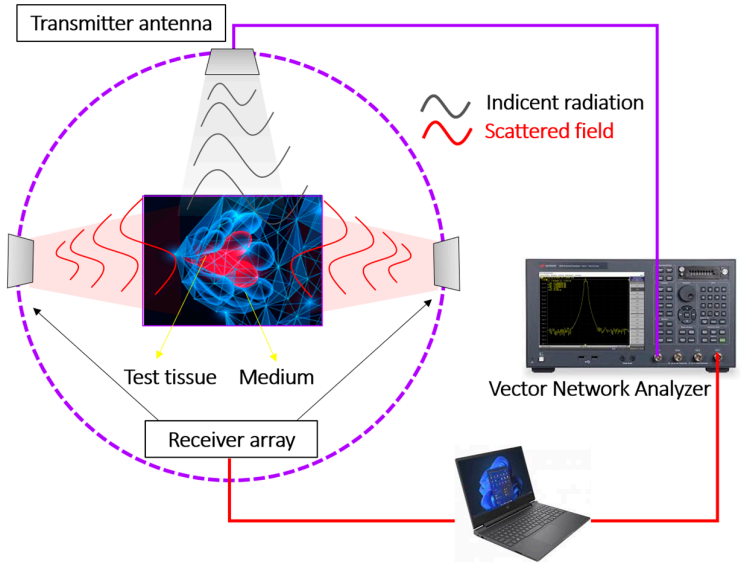

Figure 1. Simplified schematics of a microwave imaging system.

Microwaves interact with the dielectric properties (i.e. permittivity and conductivity) of biological tissues [8], then microwave imaging is based on the different dielectric properties exhibited by an abnormal cellular structure (such as a malignant tumor) in contrast to the surrounding healthy tissue. The interaction of microwaves with biological tissue causes scattered and reflected waves that are used to reconstruct an image of the desired target (i.e. tumoral region of interest).

The Debye model is usually used to simulate the biological tissue as a function of its dielectric properties, then the permittivity ε_r, is defined as [9]:

$$\varepsilon_r = \varepsilon_\infty + \frac{\varepsilon_s + \varepsilon_\infty}{1 + j\omega\tau} - j\frac{\sigma}{\omega\varepsilon_0} \quad (1)$$

where ε_s and ε_∞ are the static and permittivity at infinity frequency, σ is the conductivity and τ is the characteristic relaxation time of the medium.

The contrast mechanism of microwave tomography is based on the differences in electrical properties between normal and abnormal tissues. Microwave imaging requires solving nonlinear inverse electromagnetic scattering problems. The measurements of the scattered field allow to estimate the dielectric and conductivity parameters of biological tissues by applying non-linear inverse scattering algorithms [10–12].

Microwave imaging technique has emerged as a potential alternative to mammography methods for the early detection of breast cancer [13] and to localize and quantify the malignant lesions in a non-invasive a non-ionizing manner [14].

Furthermore, microwave imaging signals can be directly coupled to living breast tissue and then monitored for time-related changes during cancer treatment [15]. Figure 2 compares the imaging performance of regular X-ray mammography, ultrasonography and microwave tomographic imaging in breast cancer case. A visual inspection reveals clear and unequivocal detection and localization of the malignant lesion within the breast volume.

 doi:10.20944/preprints202407.1569.v1

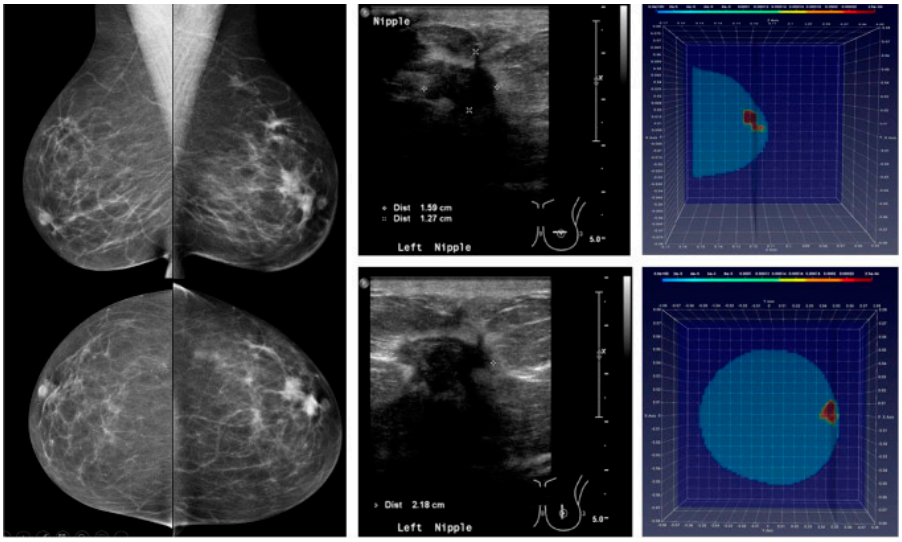

Figure 2. Mammography (left), ultrasonography (central panel) and MTI of a breast cancer patient. Reproduced from [16].

3. Raman Scattering

Raman spectroscopy is an optical scattering imaging technique that provides non-destructive analysis about chemical structure of biological tissues [17]. Raman scattering occurs upon the interaction of high-power lasers with the chemical bonds composing the biological sample. Raman scattered light undergoes a wavelength shift of the incident light whose intensity and spectrum depend on the vibrational (chemical) bond of the specific molecules. Figure 3 schematizes the Raman scattering principle: An elastic scattering event would not change the energy of the molecule and then the scattered light retains the wavelength of the incident source (i.e. Rayleigh Scattering). However, a Raman event is an inelastic scattering process in which an energy transfer occurs between the molecule and the scattered photons. If during the light-matter interaction the molecule is excited to a higher vibrational state (i.e. the molecule gains energy) the process is called Stokes Raman Scattering. On the contrary, if the molecule is relaxed to a lower vibrational state the scattered photons gain energy by increasing the wavelength, this process is known as Anti-stokes Raman Scattering [18].

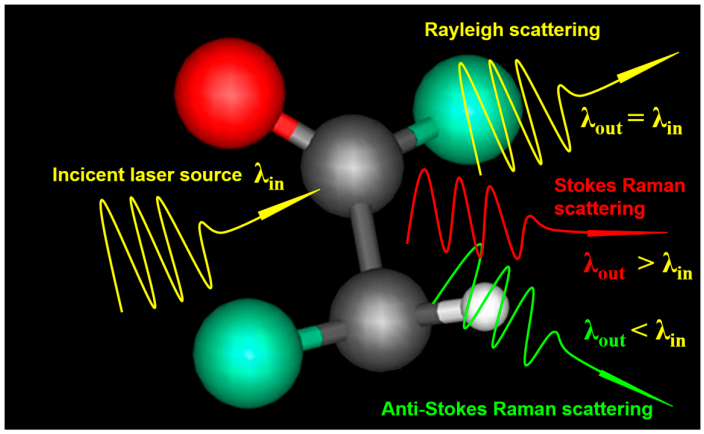

Figure 2. Raman scattering principle.

 doi:10.20944/preprints202407.1569.v1

Raman scattering shift is then related to the vibrational state of those constituent atoms, where the interaction of the external electric field $\vec{E} = E_0 \cos(\omega_0 t)$ (i.e. the laser source), with the specimen at atomic scale induces a dipole moment ($\vec{P}$) that defines the polarizability ($\bar{\bar{\alpha}}$) as [19]:

$$\bar{\bar{\alpha}} = \frac{\vec{P}}{\bar{\bar{E}}} \quad (2)$$

If the molecular polarizability is expanded into a Taylor series to the first order for a generalized coordinate $r = r_0 \cos(\omega_0 t)$:

$$\bar{\bar{\alpha}}(r) = \bar{\bar{\alpha}}_0 + \left(\frac{\partial \bar{\bar{\alpha}}}{\partial r}\right)_0 + \cdots \quad (3)$$

The scattered electric field $\vec{E}_{scatt}$ proportional to the induced dipole moment can be expressed as:

$$\vec{E}_{scatt} = \bar{\bar{\alpha}}_0 E_0 \cos(\omega_0 t) + 1/2 \left(\frac{\partial \bar{\bar{\alpha}}}{\partial r}\right)_0 r_0 E_0 [\cos(\omega_0 - \omega)\, t + \cos(\omega_0 + \omega)\, t] \quad (4)$$

In the equation (4), the first term corresponds to the elastic (Rayleigh) scattering. The second term represents the Raman scattering effect, where the shift frequencies $(\omega_0 - \omega)$ and $(\omega_0 + \omega)$ correspond to the Stokes and anti-Stokes Raman processes.

The contrast mechanism of Raman spectroscopy lies in the differences between the wavelength of incident and scattered light and therefore Raman scattering is a label-free optical technology sensitive to changes in cells and macromolecules that occurs during carcinogenesis and then a powerful tool for tumor diagnosis at molecular level [20].

Raman technology not only provides spectral information of the scattered light and information on the molecular structure of the matter studied, but also three-dimensional (3D) spatial resolution [21]. Raman scattering imaging extends classical spectroscopy to 3D visualization of the molecular structure and morphology of tumors [22] and then to the classification of types and subtypes of the malignant lesions in cancer diagnosis.

Figure 3 shows representative Raman scattering spectra from brain, primary tumor, liver, lung and spine cells. The identification and analysis of spectral regions through the Raman shift allow the discrimination of the specific malignant tissue.

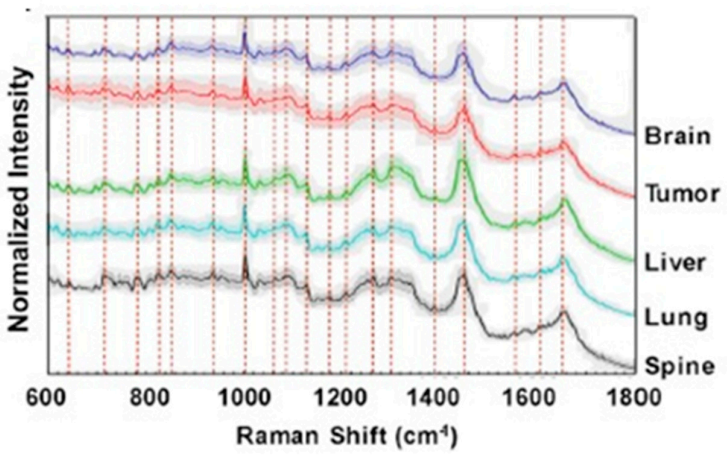

Figure 3. Normalized intensity Raman spectra for brain (blue), tumor (red), liver (green), lung (blue and spine (gray) cells. Image reproduced from [23].

Furthermore, Raman scattering offers label-free chemical imaging that has attracted interest in pharmacokinetic research due to the ability to track the biodynamics of anti-cancer drugs delivery in real-time [24]. Figure 4a shows the confocal Raman imaging spectra from confocal Raman imaging of the human hepatocellular carcinoma cell line (HepG2) in the lipids, cytoplasm and nucleus regions of the cell. Figure 4b compares the Raman spectra of HepG2 before (green spectrum) and after incubation (dark blue spectrum) with drug delivery polymers based on poly lactic-co-glycolic acid

Preprints.org (www.preprints.org) | NOT PEER-REVIEWED | Posted: 19 July 2024 doi:10.20944/preprints202407.1569.v1

nanoparticles (PLGA NPs). The pink spectrum corresponds to the PLGA NPs in dray state. The cells under study are shown in the insets.

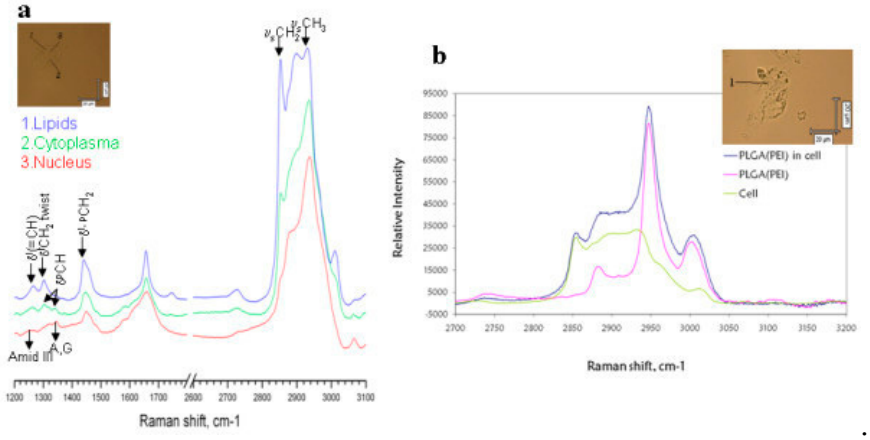

Figure 4. (a): Raman spectra of HepG2 cell line in lipids (blue), cytoplasm (green) and nucleus (red) regions. (b): Comparison of Raman spectra before (green) and after incubation of HepG2 with PLGA nanoparticles (blue). Pink spectrum corresponds to the isolated PLGA NPs. Image reproduced from [25].

Despite the benefits of Raman scattering in chemical imaging of cancer, analysis of a large volume of images and spectral data can be a tedious task. The application of deep learning algorithms to Raman scattering has made it possible to accelerate the processing, analysis, differentiation between normal and cancerous tissues and the classification [26–28] of the malignant lesions. Weng et al [29] reported a representative example of the application of artificial intelligence in Raman scattering for automatic cancer diagnosis. They reported on a deep neural network trained using Coherent anti-Stokes Raman Scattering (CARS) images from squamous cell carcinoma lung tissues. Figure 5 shows the first convolutional layer (32 kernels) in the trained model for normal (left panels) and small-cell carcinoma (right panels) CARS images. The model achieved an accuracy of 89.2 % in classifying CARS images of normal lung and carcinoma.

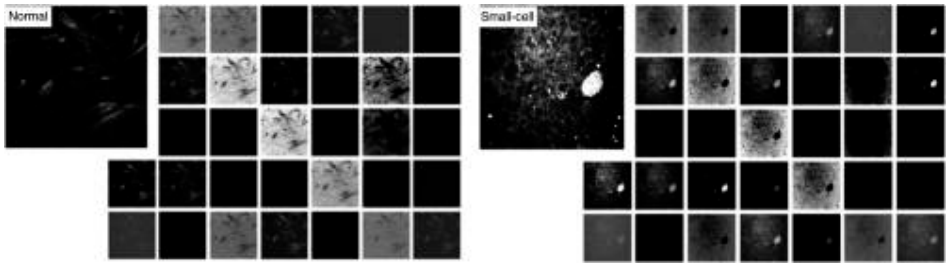

Figure 5. First convolutional layer of normal (left) and small-cell carcinoma (right) CARS images of the deep neural network trained in [29]. Images reproduced from [29].

4. Multiphoton Microscopy

Multiphoton imaging arises from the second and third-order non-linear interaction between a high-power ultra-fast infrared pulsed laser (traditionally Titanium Sapphire lasers [30]) and biological tissues [31]. When the energy addition of two or more photons allows the ground fluorophore to be excited to a higher energy excitation state, an electronic transition occurs in a manner similar to regular fluorescence [32] (single photon absorption). Then, the biological molecules in the excited state fall to the ground state with the spontaneous emission of a photon of lower energy than the sum of the incident photons due to the non-radiative vibrational relaxation process (**Figure 6**a). If two photons are absorbed, the process is known as two-photon excitation fluorescence (TPEF)

 doi:10.20944/preprints202407.1569.v1

and has the ability to produce endogenous excitation fluorescence from biomolecules such as lipofuscin, melanin, flavin and NADPH [33]. In multiphoton imaging, excitation is limited to a focal volume where the scattered light is inversely proportional to the fourth power of the wavelength of the excitation source. Furthermore, the intensity of the emission from endogenous fluorophores is proportional to the square of the excitation source; those particular characteristics provide the multiphoton imaging modality with intrinsic optical sectioning and high penetration power capabilities within scattering tissues [34].

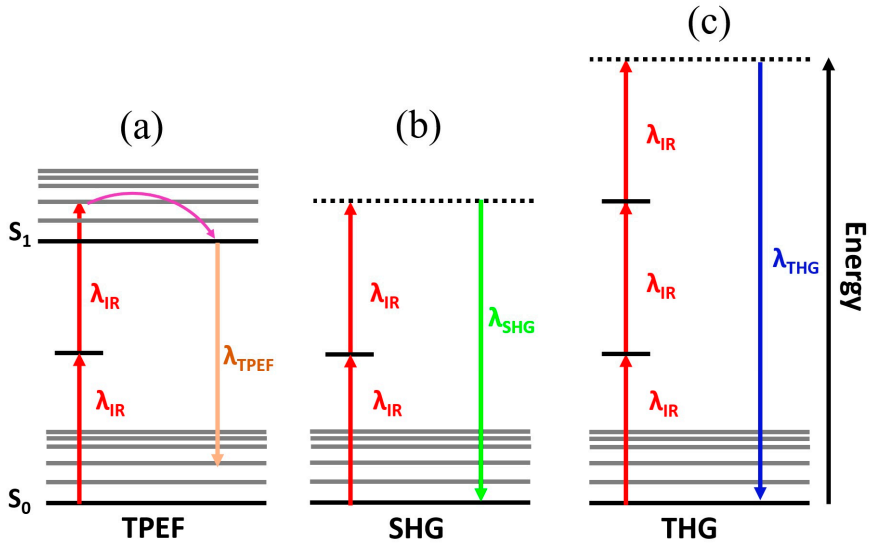

Figure 6. Illustration of the two-photon excitation fluorescence (a), second harmonic generation (b) and third harmonic generation (c) non-linear processes.

However, multiphoton microscopy is also sensitive to harmonic generations, where two or three incident photons can be instantaneously converted into a single photon with half or one-third of the excitation wavelength giving rise to second and third harmonic generation microscopy (SHG and THG) , respectively [35] (Figs. 6b and 6c). Those frequency conversion are not absorptive processes and then occur without energy dissipation as a result of excitation photons summation and phase matching induced by the nonlinear susceptibility of the biological structures [36].

The contrast mechanism of SHG and THG microscopy, unlike TPEF that requires endogenous fluorophores, arises from the frequency conversion of the incident photons due to the nonlinearity of the electromagnetic response of the specific molecular structures of biological tissues. According to the nonlinear optics theory, the excited nonlinear polarization ($\vec{P}$) is related to the excitation laser source by means of the nonlinear susceptibility, $\hat{\chi}^{(n)}$ [37]:

$$\vec{P} = \varepsilon_0 + \hat{\chi}^{(1)} \cdot \vec{E} + \hat{\chi}^{(2)} \cdot \vec{E}\,\vec{E} + \hat{\chi}^{(3)} \cdot \vec{E}\,\vec{E}\,\vec{E} + \ldots. \quad (5)$$

Therefore, the generation of harmonics depends not only on the need for ultrafast and intense pulsed laser but also on the nonlinear susceptibility of the biological tissues. The SHG signal is provided only in non-centrosymmetric media such as fibrillar collagen [38]. In contrast, THG arises from sources such as lipid-water interfaces [39] and myelinated axons [40]. Figure 6 schematizes the main multiphoton imaging modalities, which provide label-free three-dimensional visualization of biological structures at cellular scale with negligible phototoxicity. Such characteristics make multiphoton microscopy a potential tool for the analysis of tumor lesions.

4.1. Two-Photon Excitation Fluorescence Imaging

Since the experimental demonstration of the suitability of two-photon excitation fluorescence (TPEF) for biological imaging in the 90s [41], TPEF microscopy has been employed for deep tissue imaging [42], functional imaging in neurons [43], the dynamics of stromal cells interaction [44] or

 doi:10.20944/preprints202407.1569.v1

intravital subcellular imaging [45]. Subsequently, the applications of TPEF microscopy in tumor research have been expanded to tumor microenvironment, metabolism, angiogenesis and metastasis [46].

In some types of malignancy, the diagnosis usually comes at a very late stage such as gastric cancer [47]. Gastric cancer diagnosis is made by visual evaluation of gastrointestinal endoscopy and late confirmation by histopathology. However, a poor interpretation in the first (endoscopy) due to lack of obvious signs at the naked-eye, can cause a delayed impact in the second (histopathology). In that sense, TPEF microscopy allows discrimination of normal gastric tissue from cancer, adenoma or ulcers due to the capabilities of two photon imaging to visualize and measure enzymatic activity [48].

Cancer-associated fibroblasts (CAF) are cells within the tumor that promote cancer proliferation and extracellular matrix remodeling [49], and are one of the main stromal cell populations in solid tumors and contribute to drug resistance [50]. In that sense, TPEF microscopy has demonstrated the potential to analyze the structure and spatial organization of gastric cancer cells and monitoring the growth of spheroids. Figure 7 shows a single plane of TPEF images of a bicellular spheroid acquired 6 days after the start of growth.

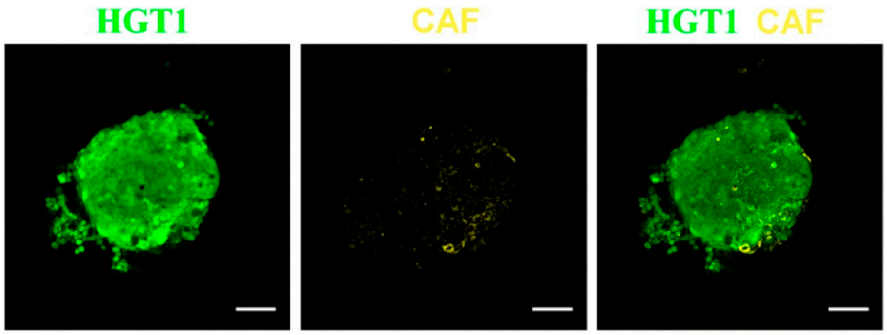

Figure 7. TPEF image of CAF (middle); monocellular HGT1 (labelled with eGFP) spheroids (left) and bicellular HGT1/CAF (right). Scale bar: 100μm. Image reproduced from [50].

Pathological assessment (i.e. histopathology) of the treatment response requires tedious and time-consuming labelling processes. As label-free imaging technique, TPEF microscopy allows the evaluation of histopathologic changes induced by neoadjuvant therapy in the preoperative stage that reveals residual tumoral cells, fibrotic reaction and inflammatory cell infiltration [51].

Tumor cells invade adjacent tissues by secreting degradative enzymes that reduces the pH of the lysosomes, then the extracellular pH of the tumoral tissues become acidic. TPEF microscopy has been proved to be pH-sensitive in the case of human colon cancer [52].

Photodynamic therapy (PDT) is a modern non-invasive light-matter based interaction method that uses photosensitizers or light-activated drugs for the treatment of non-malignant diseases and various types of cancer [53].

Once the photosensitizers are activated by a selective wavelength, a process begins for selective destruction of malignant or abnormal cells.

One of the main limitations of PDT was the photodamage induced by single-photon excitation of the photosensitizers, however the application of two-photon absorption concept made it possible to overcome this medical limitation due to the insignificant photo-toxicity of the nonlinear process that makes the technique suitable for the study of living cells [54].

The combination of two-photon excitation (TPE) and PDT gave rise to a new therapy concept (TPE-PDT) with greater penetration power into biological tissue and reduction of cells phototoxicity with promising therapeutic applications in the treatment of tumors [55].

PDT can destroy cancerous cells in inoperable types of cancer [56] or before tumors spread. PDT has been demonstrated effectiveness in the treatment of colorectal [57], lung [58], breast [59], liver and pancreatic cancer [59]. The main therapeutic mechanisms of PDT are immune response, vascular damage and direct destruction of cancer cells [60].

 doi:10.20944/preprints202407.1569.v1

4.2. Two-Photon Fluorescence Life-Time Microscopy

Lifetime TPEF microscopy measures the fluorescence decay of emission from endogenous (or exogenous) fluorophores enabling label-free *in-vivo* imaging of metabolic dynamics [61] with promising applications in infectious, neurodegenerative and cancer diseases [62].

In particular, the characterization of NAD(P)H fluorescence lifetime has been demonstrated as an intrinsic biomarker of the cellular metabolic status of living tissues capable of tracking the dynamics tumor cells [63].

In a recent publication reported by Karrobi et al [64], life-time TPEF microscopy was used to investigate changes in cellular metabolism of breast spheroids non-cancerous epithelial breast (MCF-10A) and breast cancer (MD-MB-231) cell spheroid lines embedded in collagen. The findings revealed a greater shift in cancer spheroids toward oxidative phosphorylation and how they invaded collagen over time with stronger metabolic gradient modifications than MCF-10A spheroids.

Figure 8 shows an example of time-integrated NAD(P)H two-photon excitation fluorescence image from a non-cancerous epithelial breast cell spheroid line (a) and the representative fluorescence decay signal (b).

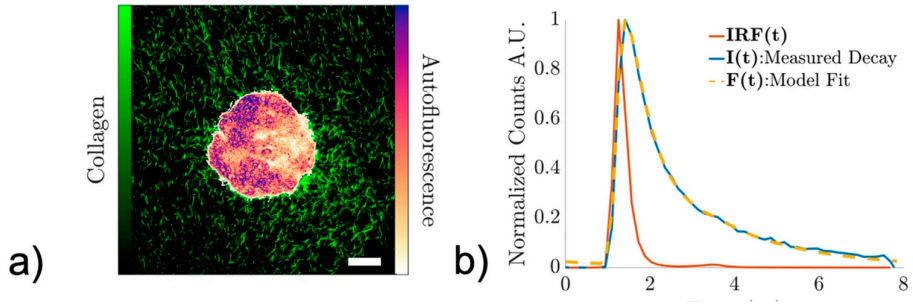

Figure 8. life-time TPEF image of a normal breast cell (a) and the normalized fluorescence decay signal (b). I(t), IRF(t) and F(t) correspond to the intensity of the decay signal, the impulse response function and a model fitted, respectively. Reproduced from [64].

Cancer cells are responsible for tumor growth and migration to other organs; however, the extracellular matrix undergoes remodeling that promotes the progression of metastasis and tumorigenesis [65]. The next subsection discusses the "gold standard" nonlinear imaging modality to visualize the extracellular matrix primarily composed of collagen [66].

4.3. Second Harmonic Generation

The extracellular matrix is not only responsible for cell maintenance, but also for cell migration [67] and proliferation [68]. In the extracellular matrix (ECM) of connective tissues, collagen is the most abundant protein [69] and plays a fundamental role in functional structure and cellular processes [70].

Type-I fibrillar collagen is organized in a non-centrosymmetric molecular structure and possesses strong nonlinear susceptibility [38]. Nowadays, second harmonic generation (SHG) microscopy (see Figure 6b for the illustration of the SHG concept) is considered the gold standard imaging technique for visualizing and characterizing collagen-formed tissues [71]. The SHG signal is endogenous, therefore the contrast mechanism arises from the structure of the sample, making this imaging technique sensitive to the molecular structure of the collagen-based connective tissue [72].

Beyond collagen-based tissues, SHG microscopy allows visualization of the structure of myosin [73], microtubules in neurons [74] or cardiomyocytes [75] when combining SHG and TPEF microscopy.

SHG signal is a coherent process with tensorial nature in which forward (F-SHG) and backward (B-SHG) emissions coexist; the ratio of F/B-SHG depends on the structure of the susceptibility tensor [76]. Therefore, SHG imaging is a powerful optical microscopy technique to analyze collagen disorders (remodeling) associated to cancer and fibrous connective tissues [77].

 doi:10.20944/preprints202407.1569.v1

In cancer progression, the ECM is remodeled alongside abnormal cells growth [78]. In particular, collagen undergoes fibrillation which induces increased stiffness in the ECM, promotes angiogenesis and cancer invasion [79]. Furthermore, changes in SHG directionality emission (i.e. the F/B-SHG ratio) has been found to be altered in bulk tumor but not in the stromal interface [80], where high values of the F/B-SHG ratio describes highly organized ECM tissues. Therefore, the characterization of spatial remodeling of collagen at the ECM is crucial as tumor invasion and metastasis are facilitated by alterations in the ECM [81].

SHG microscopy images from collagen fibers require quantitative analysis to first detect alteration in the spatial patterns and then numerically compute the collagen remodeling and degree of organization. The structure tensor, Fast Fourier transform, Wavelet or Hough transforms are well-stablished image transformation methods from which structural information can be extracted. An overview of the main image processing techniques for quantitative analysis of SHG imaging can be found in [82].

In that sense, the structure tensor [83] has been demonstrated as a useful method to quantity the organization of collagen-based tissues and classify different spatial patterns and the Hough transform was successfully used to discriminate between normal and malignant tissues, analyzing the surrounding collagen of thyroid cancer nodules capsules [84].

SHG process exhibits a strong polarization dependence [85], the polarization-sensitive nature of SHG (P-SHG) microscopy has allowed to measure the second-order nonlinear optical susceptibility tensor [86] and then obtain information about the ultrastructure of collagen. As an example, Figure 9 compares spatially-resolved components of the non-linear susceptibility tensor in normal and cancer breast tissues, obtained using P-SHG.

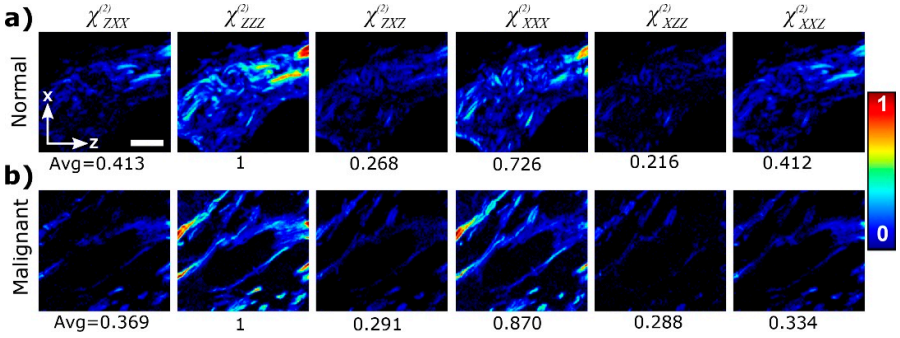

Figure 9. Second-order susceptibility values of normal (a) and tumor breast (b) tissues. Scale bar: 20 μm. Images reproduced from [92]. .

Danielle et al, [87] used P-SHG microscopy to calculate the components of the susceptibility tensor from histopathological samples of cancerous thyroid tissues, were able to measure the molecular chirality of the malignant tissues finding cancer-related collagen disorders at molecular levels.

SHG polarimetric microscopy reveals the orientation and ultrastructure of collagen that cannot be accessed by non-polarized SHG imaging. P-SHG has also been used to distinguish between breast , osteosarcoma, liver fibrosis or melanoma tissues [88–91] Therefore, pathologists can benefit from the invaluable ultrastructural information provided by polarization-sensitive SHG microscopy.

4.5. Third Harmonic Generation

While SHG microscopy arises primarily from non-centrosymmetric proteins such as type-I collagen, the third-harmonic generation (THG) signal mainly originates from interfaces between water and lipid-rich structures such as lipid droplets or membrane lipid layers [93–95]. In this non-linear process, the frequency of the excitation light triples after the interaction with biological tissue (see Figure 6) and provides information on the refractive index discontinuities of material interfaces through the third-order nonlinear susceptibility tensor $\chi^{(3)}$ [96]. In that sense, THG offers structural

 doi:10.20944/preprints202407.1569.v1

information of individual cells with submicron resolution and intracellular inhomogeneities that allows discrimination between benign and tumor tissues [97].

Figure 10 shows THG imaging of isolated cells from healthy tissue (left column) and for different grades of breast cancer. The top and bottom rows compare nuclear irregularities and nucleoli inhomogeneities. The ability of THG to detect variability in tumor cell size and shape in a non-invasive and label-free manner provides invaluable structural information from cancer biopsies at subcellular level of resolution.

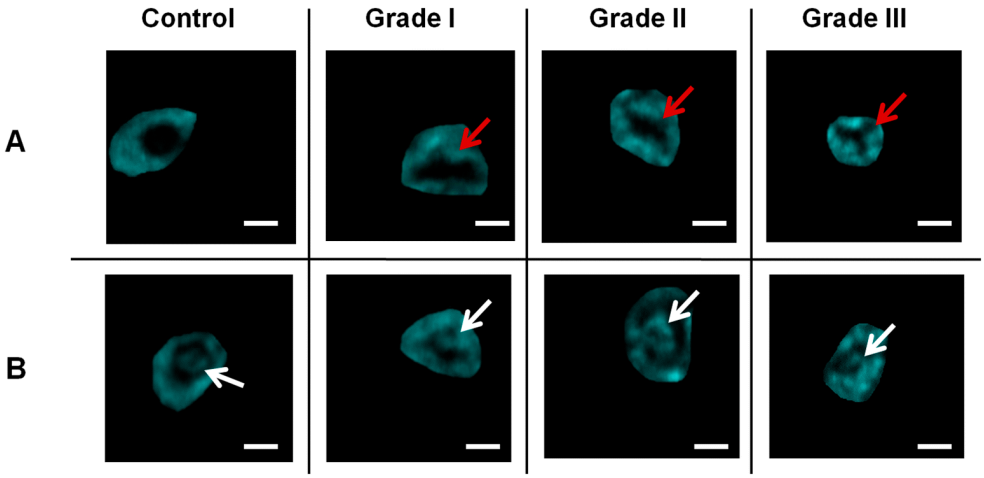

Figure 10. THG images of cells isolated from healthy (left column) and for different grades of breast cancer (third to fourth columns). The top and bottom panels compare the morphological of nucleus and nucleoli, respectively. Scale bar: 2 μm. Images reproduced from [97].

5. Digital Enhancement of the Quality of Non-Linear Imaging of Cancerous Tissues for a Better Diagnosis

Among the non-linear imaging techniques reviewed, the main goal is not only distinguish between benign and malignant tissues but also quantify the severity, aggressiveness and the outcomes of the anti-cancer treatments. Although some of the modalities offer sub-micron resolution and single cells visualization, the main common limitations lies on image contrast and resolution that allows accurate structural analysis of the pathological images.

In that sense, the image quality can be degraded by the effect of optical aberrations [98] and scattering effects [99]. Adaptive optics techniques can correct for aberrations improving the image resolution and contrast [100]. However, at deeper foci within the tissue those wavefront corrections can lose efficiency where the scattering effects increase. Or, at the time of image analysis, an AO correction equipment may not be available.

For those undesirable but possible cases, a blind image deconvolution approach for microscopy was previously developed and tested in multiphoton imaging [101].

Briefly, the algorithm performs the theoretical generation of point spread functions for spherical aberration and light scattering contributions that are employed in blind deconvolution processes in which the image is restored from those degrading factors (a detailed description of the algorithm can be found elsewhere [101]).

Hristu et al, reported a collection of multiphoton images of fixed tissues [102] involving different tissues and pathologies such as melanoma in mice, squamous cell carcinoma or breast cancer.

Here, two random images from normal and cancer breast cancer were selected to be analyzed with the algorithm to restore spherical aberration and scattering degradation factors. Figure 11 shows TPEF images of control and cancerous breast tissues (left column); naked-eye inspection reveals a less curled structure due to the ECM remodeling in the tumor tissue. The right column shows the restored images after algorithm treatment in which the image contrast, sharpness and resolution are significative increased.

 doi:10.20944/preprints202407.1569.v1

Furthermore, fine features and details are revealed to visual inspection while remain hidden in the original TPEF images. According to the basics of the algorithm, if the image quality (i.e. the sharpness, contrast or resolution) improves after processing, that image was affected by spherical aberration, scattering effects or both. For the sense of completeness, Figure 12 shows the histograms of the control and tumor images before and after algorithm processing. It can be seen how one of the algorithm effects is the equalization of the histogram, which means that the contrast of the images has been improved by distributing the intensity in the images.

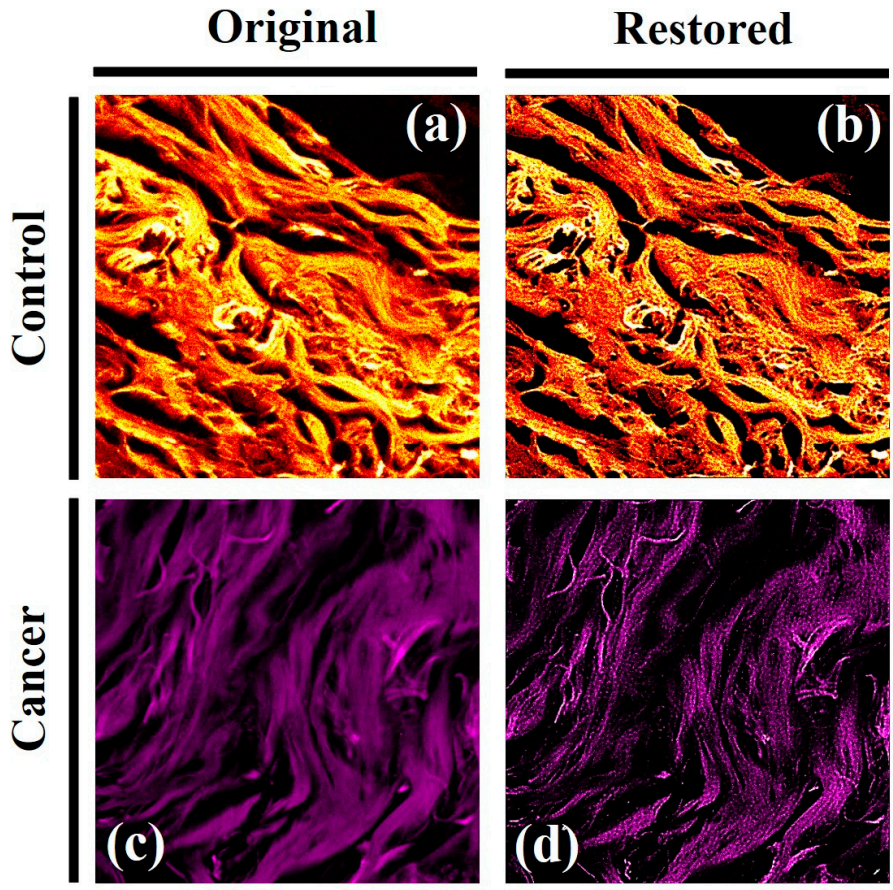

Figure 10. TPEF images of normal (a) and breast (c) cancer from fixed tissues. (c, d): results after correcting the TPEF images from spherical aberration and scattering effects. Image size: 512x512 pixels. Scanned area: 125 x 125 μm^2.

 doi:10.20944/preprints202407.1569.v1

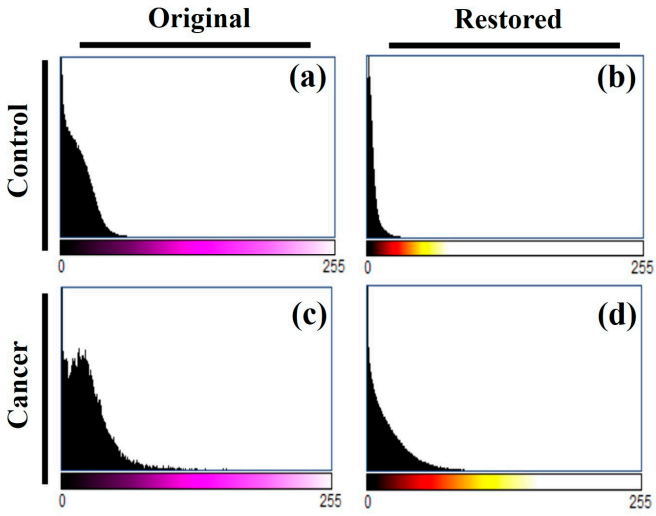

Figure 12. Histogram of TPEF images for control and cancer breast tissues (a.c) shown in **Figure 1**0, and for the restored images (b,d), respectively.

6. Discussion and Conclusions

Cancer cells exhibit non-linear optical properties that can also be considered as a predictive indicator of cellular response induced by the treatment [103]. The emergence of biocompatible nanomaterials has allowed the conversion of macroscopic analysis of tumor tissues to molecular diagnosis tools in cancer research. Nanocluster enables low-toxicity, biocompatible tumor labelling that constitute optical contrast biomarkers exhibiting nonlinear optical properties [104] that can be analyzed with the reviewed optical methods at the cellular and molecular scales. Furthermore, nanoparticles, including gold nanoparticles, protein nanoparticles, cell membrane nanoparticles quantum dots and others, can be controlled externally by optical methods, magnetism and enzymes that make them behave like smart nanoparticles that are emerging as the new era of intelligent nanoparticles cancer treatment [105].

Studying the non-linear optical properties of cancer tissues allows for rapid estimation of cellular damage or response to treatments, spatial remodeling of the ECM in cancer growth and the optimization of two-photon photodynamic therapy [106].

Furthermore, a recent study reported by Hoque et al [107] reported a promising method to detect cancer by analyzing the nonlinear optical properties of blood plasma. Their results achieved an accuracy of 92 % in discriminating between normal and cancerous samples.

In summary, cancer cells induce nonlinear optical properties in cell-matrix interaction [108] that can be measured from multimodal optical approaches that also provide invaluable monitoring of anti-cancer drugs, support the application of photodynamic therapies and the use of nanomaterials as an emerging paradigm for cancer treatment.

Funding: This research received no external funding

Institutional Review Board Statement: Not applicable.

Informed Consent Statement: Not applicable

Data Availability Statement: We encourage all authors of articles published in MDPI journals to

Acknowledgments: In this section, you can acknowledge any support given which is not covered by the author contribution or funding sections. This may include administrative and technical support, or donations in kind (e.g., materials used for experiments).

Conflicts of Interest: The author declare no conflicts of interest.

 doi:10.20944/preprints202407.1569.v1

References

1. Li, H.; Wu, J.; Xu, Q. et al. Functional genetic variants of GEN1 predict overall survival of Chinese epithelial ovarian cancer patients. J Transl Med. 2024; 22(1):577.
2. Gavgiotaki, E., Filippidis, G., Tsafas, V. et al. Third Harmonic Generation microscopy distinguishes malignant cell grade in human breast tissue biopsies. *Sci Rep* 2020; 10, 11055.
3. Winkler, J., Abisoye-Ogunniyan, A., Metcalf, K.J. et al. Concepts of extracellular matrix remodelling in tumour progression and metastasis. *Nat Commun* 2020; 11, 5120.
4. Bolomey, J.-C. and Pichot, C. Microwave tomography: From theory to practical imaging systems. Int. J. Imaging Syst. Technol. 1990; 2: 144-156.
5. Peng Z, Hwang J, Mouris J, et al. Microwave penetration depth in materials with non-zero magnetic susceptibility. ISIJ International 2010; 50(11), 1590-1596.
6. E. C. Fear, X. Li, S. C. Hagness and M. A. Stuchly, "Confocal microwave imaging for breast cancer detection: localization of tumors in three dimensions," *IEEE Transactions on Biomedical Engineering*, 2002; 49(8):812-822.
7. Tseng, C-H., Chu, T-H. An effective usage of vector network analyzer for microwave imaging. *IEEE Transactions on Microwave Theory and Techniques*, 2005; 53(9): 2884-2891.
8. Wang L. Microwave Imaging and Sensing Techniques for Breast Cancer Detection. *Micromachines*. 2023; 14(7):1462.
9. Lazebnik, M.; Okoniewski, M.; Booske, J.H.; Hagness, S.C. Highly accurate Debye models for normal and malignant breast tissue dielectric properties at microwave frequencies. IEEE Microw. Wirel. Compon. 2007, 17, 822–824.
10. Chen X., Subspace-based optimization method for solving inverse-scattering problems. IEEE Transactions on Geoscience and Remote Sensing. 2010; 48(1): 42–49.
11. Pastorino, M; Randazzo, A. Buried object detection by an inexact Newton method applied to nonlinear inverse scattering, International Journal of Microwave Science and Technology. 2012; 2012(7): 637301.
12. Liu, G. D.; Zhang, K. Y., A time-domain gauss-Newton inversion algorithm for solving two-dimensional electromagnetic inverse scattering problems, Acta Physica Sinica. 2014; 63(3): 108–122.
13. AlSawaftah, N.; El-Abed, S.; Dhou, S.; et al. Microwave Imaging for Early Breast Cancer Detection: Current State, Challenges, and Future Directions. J Imaging. 2022; ;8(5):123.
14. Moloney, B.M.; McAnena, P.F.; Abd Elwahab, S.M.; et al. Microwave Imaging in Breast Cancer - Results from the First-In-Human Clinical Investigation of the Wavelia System. Acad Radiol. 2022; Suppl 1:S211-S222.
15. Smith K, Bourqui J, Wang Z, Besler B, et al. Microwave imaging for monitoring breast cancer treatment: A pilot study. Med Phys. 2023; 50(11):7118-7129.
16. Moloney BM, McAnena PF, Abd Elwahab SM, et al. Microwave Imaging in Breast Cancer - Results from the First-In-Human Clinical Investigation of the Wavelia System. Acad Radiol. 2022; Suppl 1:S211-S22.
17. Jones, R.R., Hooper, D.C., Zhang, L. et al. Raman Techniques: Fundamentals and Frontiers. *Nanoscale Res Lett* 14, 231 (2019).
18. Kauffmann TH, Kokanyan N, Fontana MD. Use of Stokes and anti-Stokes Raman scattering for new applications. J Raman Spectrosc. 2019; 50: 418–424
19. D.J. Griffiths. Introduction to Electrodynamics (3rd Edition), , Pearson Education, Dorling Kindersley, 2007; ISBN 81-7758-293-3.
20. Qi, YF, Liu, YH, Liu, DM. Research progress on application of Raman spectroscopy in tumor diagnosis. Laser Optoelectron Prog. 2020;57(22): 220001.
21. Ilchenko O, Pilhun Y, Kutsyk A. Towards Raman imaging of centimeter scale tissue areas for real-time opto-molecular visualization of tissue boundaries for clinical applications. Light Sci Appl. 2022;11(1):143.
22. Hollon T, Orringer DA. Label-free brain tumor imaging using Raman-based methods. J Neuro-Oncol. 2021;151(3):393–402.
23. Winnard PT Jr, Zhang C, Vesuna F, Kang JW, Garry J, Dasari RR, Barman I, Raman V. Organ-specific isogenic metastatic breast cancer cell lines exhibit distinct Raman spectral signatures and metabolomes. Oncotarget. 2017;8(12):20266-20287
24. Camp, C. H., and Cicerone, M. T. Chemically sensitive bioimaging with coherent Raman scattering. *Nat. Photon.* 2015; 9 (5), 295–305.
25. Romero G, Rojas E, Estrela-Lopis I, et al. Spontaneous confocal Raman microscopy--a tool to study the uptake of nanoparticles and carbon nanotubes into cells. Nanoscale Res Lett. 2011;6(1):429.
26. Gupta S, Gupta MK, Shabaz M, Sharma A. Deep learning techniques for cancer classification using microarray gene expression data. Front Physiol. 2022;13:952709
27. Wu, M., Wang, S., Pan, S. et al. Deep learning data augmentation for Raman spectroscopy cancer tissue classification. Sci Rep. 2021; 11, 23842..
28. Blake N, Gaifulina R, Griffin LD, et al. Machine Learning of Raman Spectroscopy Data for Classifying Cancers: A Review of the Recent Literature. Diagnostics (Basel). 2022;12(6):1491.

29. Weng S, Xu X, Li J, Wong STC. Combining deep learning and coherent anti-Stokes Raman scattering imaging for automated differential diagnosis of lung cancer. J Biomed Opt. 2017; 22(10):1-10.
30. C. Lefort. A review of biomedical multiphoton microscopy and its laser sources. J Phys D: App Phys. 2017; 50(42):423001.
31. Stutzmann GE, Parker I. Dynamic multiphoton imaging: a live view from cells to systems. Physiology (Bethesda) 2005;20:15–21
32. Williams RM, Zipfel WR, Webb WW. Multiphoton microscopy in biological research. Curr Opin Chem Biol. 2001;5:603–608
33. Stringari, C., Abdeladim, L., Malkinson, G. et al. Multicolor two-photon imaging of endogenous fluorophores in living tissues by wavelength mixing. *Sci Rep* 2017; 7, 3792.
34. Centonze VE, White JG. Multiphoton excitation provides optical sections from deeper within scattering specimens than confocal imaging. Biophys J. 1998;75(4):2015-24.
35. Morizet, J., Olivier, N., Mahou, P. *et al.* Third harmonic imaging contrast from tubular structures in the presence of index discontinuity. *Sci Rep* 2023; 13, 7850.
36. R. W. Boyd, Nonlinear Optics, Academic Press (1992).
37. Lacomb R, Nadiarnykh O, Townsend SS, Campagnola PJ. Phase Matching considerations in Second Harmonic Generation from tissues: Effects on emission directionality, conversion efficiency and observed morphology. Opt Commun. 2008;281(7):1823-1832
38. Williams RM, Zipfel WR, Webb WW. Interpreting second-harmonic generation images of collagen I fibrils. Biophys J. 2005;88(2):1377-86.
39. Weigelin, B., Bakker, G.-J. & Friedl, P. Third harmonic generation microscopy of cells and tissue organization. J. Cell Sci. 2016; 129, 245–255.
40. Farrar, M. J., Wise, F. W., Fetcho, J. R. & Schaffer, C. B. In vivo imaging of myelin in the vertebrate central nervous system using third harmonic generation microscopy. Biophys. J . 2011; 100, 1362–1371.
41. Denk, W., Strickler, J. H. & Webb, W. W. Two-Photon Laser Scanning Fluorescence Microscopy. *Science* 248, 73–76 (1990).
42. Helmchen, F. & Denk, W. Deep tissue two-photon microscopy. Nat. Methods 2005; 2, 932–940.
43. Denk, W. et al. Anatomical and functional imaging of neurons using 2-photon laser scanning microscopy. J. Neurosci. Methods, 1994; 54, 151–162.
44. Bousso, P., Bhakta, N. R., Lewis, R. S. et al. Dynamics of thymocyte-stromal cell interactions visualized by two-photon microscopy. Science, 2002; 296, 1876–1880.
45. Lu Z, Zuo S, Shi M, et al. Long-term intravital subcellular imaging with confocal scanning light-field microscopy. Nat Biotechnol. 2024; 38802562.
46. Jun LIU. Two-photon microscopy in pre-clinical and clinical cancer research. Front. Optoelectron., 2015, 8(2): 141–151.
47. Kaltenmeier C., Althans A., Mascara M., et al. Pathologic complete response following neoadjuvant therapy for gastric adenocarcinoma: a national cancer database analysis on incidence, predictors, and outcomes. Am. Surg. 2021; 87(7), 1145–1154.
48. Noh CK, Lim CS, Lee GH, et al. A Diagnostic Method for Gastric Cancer Using Two-Photon Microscopy With Enzyme-Selective Fluorescent Probes: A Pilot Study. Front Oncol. 2021;11:634219.
49. Yang, D., Liu, J., Qian, H. et al. Cancer-associated fibroblasts: from basic science to anticancer therapy. *Exp Mol Med* 2023; 55, 1322–1332.
50. Alzeeb G, Dubreuil M, Arzur D, et al. Gastric cancer multicellular spheroid analysis by two-photon microscopy. Biomed. Opt. Express 2022; 13, 3120-3130.
51. Li L, Hong S, Kang D, et al.. Two-photon imaging reveals histopathological changes in the gastric tumor microenvironment induced by neoadjuvant treatment. Biomed Opt Express. 2023;14(10):5085-5096.
52. Woojung K. et al. Two-photon probes for pH: Detection of human colon cancer using two-photon microscopy. *JCO* 2018; 36, 607-607.
53. Kwiatkowski S, Knap B, Przystupski D, et al. Photodynamic therapy - mechanisms, photosensitizers and combinations. Biomed Pharmacother. 2018;106:1098-1107.
54. Benninger RKP, Piston DW. Two-photon excitation microscopy for the study of living cells and tissues. Curr Protoc Cell Biol. 2013; Chapter 4:4.11.1-4.11.24.
55. Juvekar, V.; & Lee, D.; Park, T. et al. Two-photon excitation photosensitizers for photodynamic therapy: From small-molecules to nano-complex systems. Coordination Chemistry Reviews, 2024; 506, 215711.
56. Jung, H.S.; Kim, H.J. Definitive surgery and intraoperative photodynamic therapy for locally advanced non-small cell lung cancer: A case report. World J. Surg. Oncol. 2022, 20, 265.
57. Rodrigues JA, Correia JH. Photodynamic Therapy for Colorectal Cancer: An Update and a Look to the Future. Int J Mol Sci. 2023;24(15):12204.
58. Xu, C.; Law, S.K.; Leung, A.W.N. Comparison of the Differences between Two-Photon Excitation, Upconversion, and Conventional Photodynamic Therapy on Cancers in In Vitro and In Vivo Studies. *Pharmaceuticals* 2024, *17*, 663.

 doi:10.20944/preprints202407.1569.v1

59. Starkey J; Rebane A; Drobizhev M., et al. New Two-Photon Activated Photodynamic Therapy Sensitizers Induce Xenograft Tumor Regressions after Near-IR Laser Treatment through the Body of the Host Mouse. *Clin Cancer Res* 2008; 14 (20): 6564–6573.
60. Juvekar, V.; & Lee, D.; Park, T. et al. Two-photon excitation photosensitizers for photodynamic therapy: From small-molecules to nano-complex systems. Coordination Chemistry Reviews, 2024; 506, 215711.
61. Bower AJ; Li J; Chaney EJ, et al. High-speed imaging of transient metabolic dynamics using two-photon fluorescence lifetime imaging microscopy. Optica 2018; 5, 1290-1296.
62. Ranawat H, Pal S, Mazumder N. Recent trends in two-photon auto-fluorescence lifetime imaging (2P-FLIM) and its biomedical applications. Biomed Eng Lett. 2019;9(3):293-310.
63. Liang W; Chen D; Guan H, et al. Label-Free Metabolic Imaging In Vivo by Two-Photon Fluorescence Lifetime Endomicroscopy. ACS Photonics 2022; 9 (12), 4017-4029.
64. Karrobi, K., Tank, A., Fuzail, M.A. et al. Fluorescence Lifetime Imaging Microscopy (FLIM) reveals spatial-metabolic changes in 3D breast cancer spheroids. Sci Rep 2023; 13, 3624.
65. Winkler, J., Abisoye-Ogunniyan, A., Metcalf, K.J. et al. Concepts of extracellular matrix remodelling in tumour progression and metastasis. *Nat Commun* 2020; 11, 5120.
66. Frantz C, Stewart KM, Weaver VM. The extracellular matrix at a glance. J Cell Sci. 2010;123(24):4195-200.
67. Hynes RO. The extracellular matrix: not just pretty fibrils. Science 2009; 326: 1216–1219.
68. Pelham RJ, Wang Y-L. Cell locomotion and focal adhesions are regulated by substrate flexibility. Proc Natl Acad Sci USA 1997; 94: 13661–13665.
69. Tanzer ML. Current concepts of extracellular matrix. J Orthop Sci 2006; 11: 326–331.
70. Rozario T, DeSimone DW. The extracellular matrix in development and morphogenesis: a dynamic view. Dev Biol 2010; 341: 126–140.
71. Xydias D, Ziakas G, Psilodimitrakopoulos S, Lemonis A, Bagli E, Fotsis T, Gravanis A, Tzeranis DS, Stratakis E. Three-dimensional characterization of collagen remodeling in cell-seeded collagen scaffolds via polarization second harmonic generation. Biomed Opt Express. 2021;12(2):1136-1153.
72. Aghigh A, Bancelin S, Rivard M, Pinsard M, Ibrahim H, Légaré F. Second harmonic generation microscopy: a powerful tool for bio-imaging. Biophys Rev. 2023;15(1):43-70.
73. Mohler W, Millard AC, Campagnola PJ. Second harmonic generation imaging of endogenous structural proteins. Methods. 2003;29:97–109.
74. Jiang J, Yuste R. Second-harmonic generation imaging of membrane potential with photon counting. Microsc Microanal off J Microsc Soc Am Microbeam Anal Soc Microsc Soc Can. 2008;14:526–531.
75. Wallace SJ, Morrison JL, Botting KJ, Kee TW. Second-harmonic generation and two-photon-excited autofluorescence microscopy of cardiomyocytes: quantification of cell volume and myosin filaments. J Biomed Opt. 2008;13:064018.
76. Liu, J; Ying, J ; Hanping, L. et al. The forward and backward second-harmonic generation from crystallized collagen fibre with tightly focused linearly polarized beams Journal of Optics, 2012; 14(5): 055301.
77. Keikhosravi A, Bredfeldt JS, Sagar AK, Eliceiri KW. Second-harmonic generation imaging of cancer. Methods Cell Biol. 2014;123:531-46.
78. Winkler J., Abisoye-Ogunniyan A., Metcalf K.J., Werb Z. Concepts of extracellular matrix remodelling in tumour progression and metastasis. Nat. Commun. 2020;11:5120.
79. Song K, Yu Z, Zu X, Li G, Hu Z, Xue Y. Collagen Remodeling along Cancer Progression Providing a Novel Opportunity for Cancer Diagnosis and Treatment. Int J Mol Sci. 2022;;23(18):10509.
80. Desa DE, Wu W, Brown RM, Brown EB 4th, Hill RL, Turner BM, Brown EB 3rd. Second-Harmonic Generation Imaging Reveals Changes in Breast Tumor Collagen Induced by Neoadjuvant Chemotherapy. Cancers (Basel). 2022;14(4):857
81. Venning, F. A., Wullkopf, L., and Erler, J. T. Targeting ECM disrupts cancer progression. Front. Oncol. 2015; 5, 224.
82. Nejim, Z., Navarro, L., Morin, C. et al. Quantitative analysis of second harmonic generated images of collagen fibers: a review. Res. Biomed. Eng. 2023; 39, 273–295.
83. Avila, F.; Bueno JM. collagen organization with the structure tensor in second harmonic microscopy images of ocular tissues. Appl Opt. 2015;54(33):9848-54.
84. Bueno JM, Ávila FJ, Hristu R, Stanciu SG, Eftimie L, Stanciu GA. Objective analysis of collagen organization in thyroid nodule capsules using second harmonic generation microscopy images and the Hough transform. Appl Opt. 2020; 59(23):6925-6931.
85. Alizadeh M, Ghotbi M, Loza-Alvarez P, Merino D. Comparison of Different Polarization Sensitive Second Harmonic Generation Imaging Techniques. Methods Protoc. 2019;2(2):49.
86. Yu W, Li X, Wang B, et al. Nonlinear polarization tensor measurement with a vectorial complex field in second-harmonic-generation microscopy Phys. Rev. A 2023; 107, 013505.
87. Tokarz, D., Cisek, R., Joseph, A. et al. Characterization of pathological thyroid tissue using polarization-sensitive second harmonic generation microscopy. Lab Invest, 2020; 100, 1280–1287.

88. Hompland T, Erikson A, Lindgren M, et al.. Second-harmonic Generation in Collagen as a Potential Cancer Diagnostic Parameter. *J Biomed Opt.* 2008; 13:054050
89. Rouède D, Schaub E, Bellanger J-J, et al. Determination of Extracellular Matrix Collagen Fibril Architectures and Pathological Remodeling by Polarization Dependent Second Harmonic Microscopy. *Sci Rep.* 2017; 7:12197.
90. Ambekar R, Lau T-Y, Walsh M, et al. Quantifying Collagen Structure in Breast Biopsies Using Second-Harmonic Generation Imaging. *Biomed Opt Express,* 2012; 3:2021–35.
91. Lin J, Pan S, Zheng W, Huang Z. Polarization-resolved Second-Harmonic Generation Imaging for Liver Fibrosis Assessment without Labeling. *Appl Phys Lett* 2013; 103:173701.
92. Golaraei A, Kontenis L, Cisek R, et al. Changes of collagen ultrastructure in breast cancer tissue determined by second-harmonic generation double Stokes-Mueller polarimetric microscopy. Biomed. Opt. Express 2016; 7, 4054-4068.
93. Gavgiotaki E, Filippidis G, Markomanolaki H, et al. Distinction between breast cancer cell subtypes using third harmonic generation microscopy. J Biophotonics. 2017;10(9):1152-1162.
94. Aptel F, Olivier N, Deniset-Besseau A, et al.Multimodal Nonlinear Imaging of the Human Cornea. *Invest. Ophthalmol. Vis. Sci.* 2010;51(5):2459-2465
95. Watanabe, T., Thayil, A., Jesacher, A. et al. Characterisation of the dynamic behaviour of lipid droplets in the early mouse embryo using adaptive harmonic generation microscopy. BMC Cell Biol 2010; 11, 38.
96. Müller, M., Squier, J., Wilson, K. et al. 3D microscopy of transparent objects using third-harmonic generation. J. Microsc.1998;191, 266-274.
97. Gavgiotaki, E., Filippidis, G., Tsafas, V. et al. Third Harmonic Generation microscopy distinguishes malignant cell grade in human breast tissue biopsies. Sci Rep 2020; 10, 11055.
98. Zhang Q, Hu Q, Berlage C, et al. Adaptive optics for optical microscopy [Invited]. Biomed Opt Express. 2023;14(4):1732-1756.
99. Yoon S., Kim M., Jang M., et al. Deep optical imaging within complex scattering media. Nat. Rev. Phys. 2020; 2(3), 141–158.
100. Sinefeld D., Paudel H. P., Ouzounov D. G., et al. Adaptive optics in multiphoton microscopy: comparison of two, three and four photon fluorescence. Opt. Express 2015; 23(24), 31472.
101. Ávila, F.J.; Bueno, J.M. Spherical Aberration and Scattering Compensation in Microscopy Images through a Blind Deconvolution Method. *J. Imaging* 2024, *10*, 43.
102. Hristu, R., Stanciu, S.G., Dumitru, A. et al. PSHG-TISS: A collection of polarization-resolved second harmonic generation microscopy images of fixed tissues. Sci Data 2022; 9, 376.
103. Ardakani AA, Ghader A, Asgari H, et al. The capability of nonlinear optical characteristics as a predictor for cellular uptake of nanoparticles and cell damage. Photodiagnosis Photodyn Ther. 2019;27:442-448.
104. Combes GF, Vučković AM, Perić Bakulić M, et al. Nanotechnology in Tumor Biomarker Detection: The Potential of Liganded Nanoclusters as Nonlinear Optical Contrast Agents for Molecular Diagnostics of Cancer. Cancers (Basel). 2021;13(16):4206.
105. Sun, L., Liu, H., Ye, Y., et al. Smart nanoparticles for cancer therapy. Sig Transduct Target Ther. 2023;8, 418.
106. V.M. Aneesa, K.P. Safna, Hussan, S. et al.Analysis of non-linear optical properties of phytochemical photosensitizers in cancer photodynamic therapy by quantum computational Results in Chemistry, 2024; 8, 101580,
107. Hoque, E; Biswas, M; Hossain M, et al. Nonlinear optical phase shift in blood plasmas for neoplasia diagnosis. Opt. Express 2023; 31, 23056-23065
108. Ghader A, Behruzi M, Majles Ara MH, Ghaznavi H, Abbasian Ardakani A. Nonlinear optical response of cancer cells following conventional and nano-technology based treatment strategies: Results of chemo-, thermo- and radiation therapies. Photodiagnosis Photodyn Ther. 2022;37:102686.